Arabian Journal of Chemistry (2020) 13, 5526–5538

King Saud University

Arabian Journal of Chemistry

www.ksu.edu.sa
www.sciencedirect.com

ORIGINAL ARTICLE

Magnesium-containing silk fibroin/polycaprolactone electrospun nanofibrous scaffolds for accelerating bone regeneration

Xin Xing [a,1], Gu Cheng [a,b,1], Chengcheng Yin [a], Xin Cheng [a], Yuet Cheng [a], Yifeng Ni [a], Xue Zhou [c], Hongbing Deng [b,*], Zubing Li [a,*]

[a] *The State Key Laboratory Breeding Base of Basic Science of Stomatology (Hubei-MOST) and Key Laboratory of Oral Biomedicine Ministry of Education, School and Hospital of Stomatology, Wuhan University, Wuhan 430079, China*
[b] *Hubei International Scientific and Technological Cooperation Base of Sustainable Resource and Energy, Hubei Key Lab of Biomass Resource Chemistry and Environmental Biotechnology, School of Resource and Environmental Science, Wuhan University, Wuhan 430079, China*
[c] *School of Public Health, Tongji Medical College, Huazhong University of Science and Technology, Wuhan 430030, China*

Received 17 February 2020; accepted 31 March 2020
Available online 6 April 2020

KEYWORDS

Magnesium;
Silk fibroin;
Polycaprolactone;
Nanofibrous scaffolds;
Bone regeneration

Abstract Bone tissue engineering has become one of the most effective methods for treating bone defects. In this study, an electrospun tissue engineering membrane containing magnesium was successfully fabricated by incorporating magnesium oxide (MgO) nanoparticles into silk fibroin and polycaprolactone (SF/PCL)-blend scaffolds. The release kinetics of Mg^{2+} and the effects of magnesium on scaffold morphology, and cellular behavior were investigated. The obtained Mg-functionalized nanofibrous scaffolds displayed controlled release of Mg^{2+}, satisfactory biocompatibility and osteogenic capability. The in vivo implantation of magnesium-containing electrospun nanofibrous membrane in a rat calvarial defect resulted in the significant enhancement of bone regeneration twelve weeks post-surgery. This work represents a valuable strategy for fabricating functional magnesium-containing electrospun scaffolds that show potential in craniofacial and orthopedic applications.

* Corresponding authors.
E-mail addresses: hbdeng@whu.edu.cn (H. Deng), lizubing@whu.edu.cn (Z. Li).
[1] Contributed equally to this work.

Peer review under responsibility of King Saud University.

Production and hosting by Elsevier

1. Introduction

Bone defects caused by infection, trauma and tumour are common, and the clinical management of their repairs remains a challenging task (Roddy et al., 2018). Traditional clinical approaches involve allografts, autografts and distraction osteogenesis, which may provide positive effects but suffer from shortcomings, such as donor site morbidity, immune

https://doi.org/10.1016/j.arabjc.2020.03.031
1878-5352

complications and cosmetic concerns (Lauthe et al., 2018). To date, many bone substitutes, defined as synthetic, inorganic or biologically organic combinations, which can be inserted for the treatment of bone defects, can fill bone defects to overcome these limitations (Fernandez de Grado et al., 2018). Among these materials, the use of synthetic bone tissue engineering scaffolds is becoming increasingly popular (Winkler et al., 2018).

Silk fibroin (SF), a natural protein, has good biocompatibility and tunable biodegradability (Cheng et al., 2018). Silk-based biomaterials are considered potential resources for tissue regeneration, especially bone tissue engineering (Bhattacharjee et al., 2017). The use of silk-based scaffolds for bone-tissue engineering is attractive because of their easy and flexible processing. Various processing and modification strategies for silk-based scaffolds include electrospinning, freeze drying, 3D printing, surface engineering, and mineralization (Bhattacharjee et al., 2017; Chen et al., 2018; Choi et al., 2018; Rödel et al., 2018). Electrospinning is extensively used because it is easy to operate, relatively inexpensive, and versatile. More importantly, the electrospun nano-sized fibres have superior performance compared to micro-scale fibres (Farokhi et al., 2020). Composites with desirable properties can be designed by blending silk with synthetic polymers to achieve suitable strength and degradation. PCL has better mechanical properties and longer absorption times than SF (Kim et al., 2015). Recently, we successfully fabricated an electrospun membrane that combines SF and PCL and exhibits excellent mechanical and biocompatibility properties (Cheng et al., 2018). By adjusting the ratio of SF and PCL, the degradation time of the SF/PCL composite membrane can also be adjusted to be in coordination with bone healing time.

The incorporation of bioactive substances in bone-tissue engineering scaffolds is a valuable application in this field. Magnesium (Mg) is the fourth most common metal element in the human body and plays an important role in mineral metabolism (Grober et al., 2015). About 60% of the entire body's Mg is stored in bone tissue (Castiglioni, 2013). Moreover, Mg ions can be absorbed into the lattice of bone minerals, such as hydroxyapatite, and influence bone density and biomechanical properties (Zhang et al., 2017; Zhang et al., 2016). Mg has elicited substantial scholarly attention worldwide over the past years. Numerous reports have demonstrated that magnesium can regulate cell adhesion and differentiation and accelerate mineralisation to stimulate local bone formation and healing (Burmester et al., 2017; Wu et al., 2015; Kim et al., 2017; Lin et al., 2019; Terranova et al., 2016). Several studies that used Mg metal/alloys as biomaterials for bone healing have revealed the potential biomedical applications of such materials (Choi et al., 2018; Farokhi et al., 2020; Adhikari et al., 2019; Yoshizawa et al., 2015; Kim et al., 2018; Yu et al., 2019). However, the rapid degradation rates under physiological conditions and the by-product hydrogen gas around the implantation sites lead to undesirable results in bone regeneration (Noviana et al., 2016; Seitz, 2014).

Mg ions (Mg^{2+}) are selected as an alternative supply to avoid the drawbacks of Mg metal/alloys. Yin et al. added $MgSO_4$ to a photo-cross-linked alginate hydrogel to achieve Mg^{2+}-incorporated alginate hydrogels that exert potential effects on the proliferation and differentiation of osteoblasts (Yin et al., 2015). Roh et al. investigated the effects of adding MgO nanoparticles to polycaprolactone /hydroxyapatite (PCL/Hap) composites fabricated with a 3D bioextruder and found that MgO and Hap addition to the 3D PCL scaffold positively influences pre-osteoblast cell behaviours, such as initial adhesion, proliferation and differentiation (Roh et al., 2017). Yuan et al. prepared poly(lactide-co-glycolide) (PLGA) microspheres co-embedded with MgO and $MgCO_3$ and discovered that bioresorbable microspheres with controlled Mg^{2+} release features are efficient in treating bone defects (Yuan et al., 2019). The controlled delivery of Mg^{2+} ions via a suitable scaffold may be an effective means to promote bone regeneration.

Electrospinning technology has been applied as an effective tool to fabricate scaffolds with a structure similar to that of native extracellular matrix and advantages, such as high surface area-to-volume ratios (Haider et al., 2018). Suryavanshi et al. fabricated an MgO-loaded electrospun PCL fibre and showed good in-vitro biological performance in terms of mineralization, degradation, and biocompatibility. On subcutaneous implantation, the scaffold revealed initial moderate inflammatory tissue response near implant site at two-week timepoint that subsided eighth week later without any vital organ toxicity (Suryavanshi et al., 2017). In this work, we incorporated MgO nanoparticles into SF/PCL composite scaffold through blend electrospun technology to prepare a functional magnesium-containing nanofibrous membrane. The characterisation properties of composite nanofibrous membranes and their effects on pre-osteoblast behaviours, including cytotoxicity, attachment and osteogenic differentiation, were investigated. To the best of our knowledge, the bone repair potential of this magnesium-containing SF/PCL electrospun material has not been confirmed with in any animal models of bone defects. In this study, the magnesium-incorporated composite electrospun membranes were covered on full-thickness rat calvarial defects and in vivo bone healing was assessed radiographically and histologically (Scheme 1). We believe that this functional magnesium-containing SF/PCL composite electrospun scaffold can be used as a potential bone graft especially suitable for bone defect repairing.

2. Experimental

2.1. Fabrication of Mg-containing SF/PCL electrospun nanofibrous membranes

SF (Cellamatrix Co., Ltd., China) and PCL (70,000–90,000 DA Sigma-Aldrich, St Louis, MO, USA) were dissolved separately in hexafluoroisopropanol (HFIP) under magnetic stirring for 24 h. A solution mixture consisting of SF and PCL with a weight ratio of 4:1 was prepared as reported in our previous study (Cheng et al., 2018). Magnesium oxide nanoparticles (Sigma-Aldrich, St Louis, MO, USA) were manually mixed into the SF/PCL solution at different concentrations of 15 wt%, 20 wt% and 25 wt%. The electrospinning process adopted the same parameters used in a previous study (Cheng et al., 2018). A high DC voltage of 16 kV was applied to set up an electric field, and the distance between the collector and spinneret was 12 cm. The solution flow rate and rotary collector speed were maintained at 1 mL/h and 300 rpm, respectively.

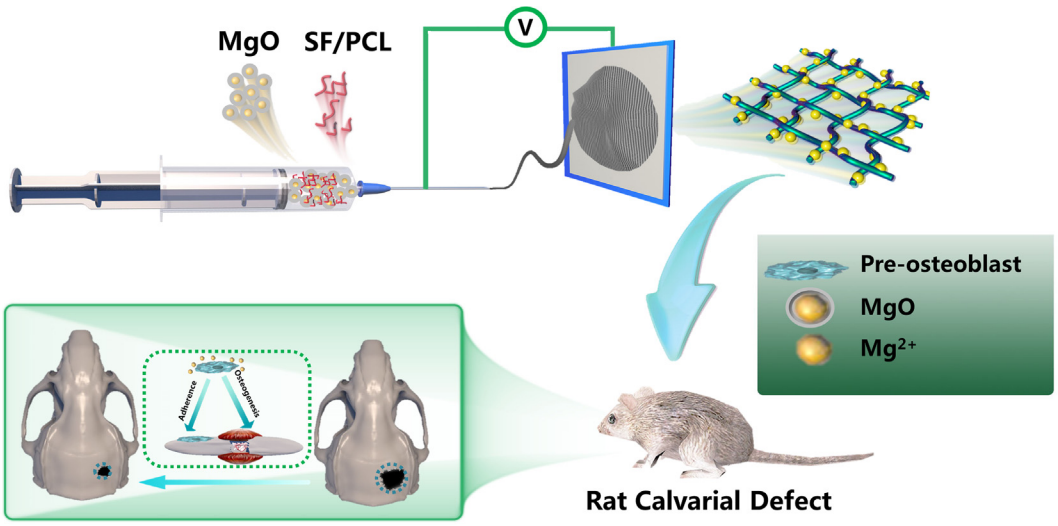

Scheme 1 MgO nanoparticles incorporated-SF/PCL electrospun nanofibrous membrane release Mg^{2+} to promote pre-osteoblast adherence, osteogenic differentiation and accelerate bone regeneration in a rat calvarial defect.

2.2. Characterisation of SF/PCL/MgO electrospun membranes

Fibre morphology was observed with a scanning electron microscope (SEM ZEISSΣ SIGMA, Germany). The mean diameters of the nanofibres for each electrospinning membrane were calculated by counting 100 different fibres from the SEM photographs using Image J software. An Axis Ultra DLD apparatus (Kratos, UK) was used for X-ray photoelectron spectroscopy (XPS) to investigate the atomic composition of the SF/PCL/MgO electrospun membranes. Water contact angles (WCA) were determined with a CASTR 3.0 drop shape analysis system (USA KINO Industry Co., Ltd., USA).

2.3. Cell adhesion

The fibrous membranes were shaped into round pieces with different diameters that were suitable for placing into different cell culture plates. The tablet diameter for SEM analysis was 14 mm and fit into 24-well plates. All of the scaffold tablets underwent sterilisation under ultraviolet light for at least 12 h before cell seeding. The MC3T3-E1 pre-osteoblasts were inoculated on the nanofibrous membrane in a 24-well plate at a density of 5×10^5/well. After 3 and 10 days of culture, the cells were washed with PBS and fixed with 3% glutaraldehyde. Following three rinses with PBS, the cellular scaffolds were dehydrated using graded ethanol and freeze dried for SEM observation. For confocal fluorescence microscope observation, the cells were incubated onto the electrospun fibrous membranes for three days then fixed and stained for actin filaments and nucleus with FITC conjugated phalloidin and DAPI, respectively. The stained compounds were examined under a confocal fluorescence microscope (Olympus, Japan) to evaluate the cell attachment.

2.4. Controlled release of Mg^{2+}

20 mg SF/PCL electrospun membranes were soaked in 10 mL of PBS and incubated at 37 °C to determine the release behaviour of Mg^{2+}. On days 1, 2, 3, 5, 7, 10, 14, 20, 25 and 30, the supernatant (1 mL) was collected. Mg^{2+} concentration was ascertained according to the manual instruction of the Mg assay kit (BioAssay Systems, CA, USA). Fresh PBS (1 mL) was replenished after the supernatant was removed to continue the release. Three parallel measurements were obtained at each time point for averaging.

2.5. Cytotoxicity evaluation

To evaluate the cytotoxicity of the electrospun nanofibrous membranes, we incubated 20 mg scaffolds in 10 mL α-MEM supplemented with 10% FBS for 15 days to obtain extracts. The MC3T3-E1 cells were seeded onto 96-well plates at a density of 5×10^3/well. After cell adherence, the culture media were replaced by extracts with different dilution ratios (0, 25%, 50%, 75%, 100%). The extracts were removed after 1, 3, 5 and 7 days of culture, and CCK-8 solutions (10% in α-MEM) were added to each well at 37 °C in 5% CO_2 for three hours. The supernatant was collected afterwards, and the optical density was measured with a microplate reader at 450 nm.

2.6. In vitro osteogenic differentiation analysis

Alkaline phosphatase (ALP) activity analysis and alizarin red S staining were conducted to determine the osteogenic differentiation property of the scaffolds. MC3T3-E1 cells were seeded onto 24-well plates or scaffold tablets at a density of 3×10^4/well. After 24 h, the culture media were replaced with osteogenic media (50 μg/mL of ascorbic acid-2 phosphate, 10 mM of β-glycerophosphate and 10 nM of dexamethasone in α-MEM containing 10% FBS and 1% penicillin–streptomycin) that included the extracts from scaffolds soaked for 15 days. ALP staining was performed at the end of the 14th day time point after replacing with osteogenic media according to the manufacturers' protocols of the ALP assay kit (Nanjing, Jiancheng, China). For the ALP quantitative analysis, the cells were lysed with 1% TritonX-100, 50 μL of p-nitrophenyl phosphate substrate solution, 80 μL of glycine buffer and 50 μL of cell lysate, all of which were added to a 96-well plate. Then, the

mixture was incubated for 30 min, and the absorbance was measured at 405 nm after adding 20 μ L of stop solution (5 M NaOH).

The mineralisation associated with osteoblastic activity was assessed through alizarin red S staining after 21 days of incubation. The cells or compounds were washed twice with PBS and fixed by 4% paraformaldehyde for 20 min. Upon washing with distilled water, 1% alizarin red S solution in Tris-HCl at pH 4.2 was added to each well and incubated for 30 min. The cells were viewed and photographed after rinsing with distilled water. Subsequently, cetylpyridinium chloride (Sigma-Aldrich, St Louis, MO, USA) was used to dissolve the mineralised nodules, and the absorbance at 562 nm was ascertained using a microplate reader.

2.7. Gene expression

After seven days of culture, the expression of osteogenesis-related genes, including BMP2, OCN, ALP and RUNX2, was examined via quantitative real-time polymerase chain reaction (PCR). Briefly, the cells/membrane compounds were ground in a mortar and sonicated after freezing in liquid nitrogen. Total RNA was isolated from the extract obtained with TRIzol reagent (Invitrogen, USA). A kit for complementary DNA (cDNA) synthesis (TAKARA, Shiga, Japan) was utilised to produce cDNA after purifying the total RNA. Quantitative real-time PCR was performed using an SYBR Green Master Mix kit (TAKARA, Shiga, Japan) in an ABI PRISM 7500 system (Applied Biosystems) in accordance with the manufacturer's protocols. The primers (reverse and forward) were shown in Table 1. The cycle threshold (CT) was utilised to determine the copy numbers of genes. Glyceraldehyde-3-phosphate dehydrogenase (GAPDH) was used as the normalised standard and internal control to obtain the $2^{-\Delta\Delta}$ Ct value expressed as a relative fold expression.

2.8. Animal model of in vivo calvarial defects

Twenty-four male Sprague Dawley rats (male, 8 weeks old, 180 g on the average) from the Hubei Provincial Laboratory Animal Center were used in this study. The animal handling and surgical protocols were conducted according to the guidelines for animal care and use committee of Wuhan University, People's Republic of China, and approved by the Ethics Committee at the School and Hospital of Stomatology. The rats were randomly divided into the control (n = 8), SF/PCL group (n = 8) and SF/PCL/MgO group (n = 8). After administering anaesthesia with pentobarbital sodium through intraperitoneal injection, a sagittal incision along the midshaft was created to expose the cranial bone. Full-thickness calvarial defects with diameters of 5 mm were created symmetrically on both sides of the middle ridge by using a trephine. After covering different membranes, the incisions were sutured for closure. The rats were given free access to food and water after surgery, and each animal was administered 4×10^4 IU of penicillin for three days by intramuscular injection.

2.9. μ-computed tomography (μ-CT) and histology imaging

The rats were sacrificed 4, 8 and 12 weeks after surgery, and the tissues were fixed in 10% formaldehyde. μ-CT imaging was performed with a ninspeXioSMX100CT system (BRUKER, USA) to obtain 3D reconstructed images. The value of bone volume/total bone volume (BV/TV) was calculated. After scanning, the samples were decalcified in 10% EDTA, dehydrated in graded ethanol series, embedded in paraffin and sectioned at 5 μm thickness for staining. Hematoxylin and eosin (H&E) and Masson's trichrome staining were adopted for histological observation.

3. Results

3.1. Morphological characterisation of the SF/PCL/MgO membrane

Given that natural bone tissue contains a large portion of inorganic and organic components, many inorganic materials, such as Mg, are effective for biomedical applications and have been incorporated into polymer scaffolds. Our previous work confirmed that when the SF-to-PCL ratio is 4:1, electrospun fibres obtain a suitable uniform diameter, surface wettability and sufficient tensile strength (Cheng et al., 2018). In this present research, MgO nanoparticles were introduced to the SF/PCL commixture to fabricate SF/PCL/MgO composite membranes. The internal structures of each SF/PCL/MgO membrane functioning with different ratios of MgO nanoparticles were examined through SEM. When the weight-to-volume ratio of MgO was 15%, the electrospun nanofibres displayed small interspaces, irregular fibre morphology, disorderly arrangement and aggregation of nanoparticles (Fig. 1**a**). When the MgO ratio was increased to 25 wt%, excessive Mg salt particles were observed on the nanofibres. The average fibre diameters of 15 wt% SF/PCL/MgO, 20 wt% SF/PCL/MgO and 25 wt% SF/PCL/MgO were 651 ± 165 nm, 1055 ± 171 nm and 1251 ± 240 nm, respectively (Fig. 1**b**). With the increase in MgO nanoparticles content, the diameters of the SF/PCL/MgO electrospinning nanofibres gradually increased. The 20 wt% SF/PCL/MgO electrospinning nanofibrous mats were selected for the follow-up experiments. Component analysis via XPS (Fig. 1**c**) indicated a typical absorption peak of Mg at 1303.6 eV, suggesting the successful incorporation of Mg (Aksoy et al., 2012).

Table 1 Primer sequences used in the qRT-PCR.

Primer	Forward 5′-3′	Reverse 5′-3′
BMP2	AAGCGTCAAGCCAAACACAAAC	GCCACGATCCAGTCATTCCAC
RUNX2	ACCAGATGGGACTGTGGTTA	AAGGTGAAACTCTTGCCTCG
OCN	CGCTCTGTCTCTCTGACCTC	GACTGAGGCTCCAAGGTAGC
ALP	TGAGCGACACGGACAAG	CTGGTAGTTGTTGTGAGCGTAA
GAPDH	AGAAGGTGGTGAAGCAGGCATC	CGAAGGTGGAAGAGTGGGAGTTG

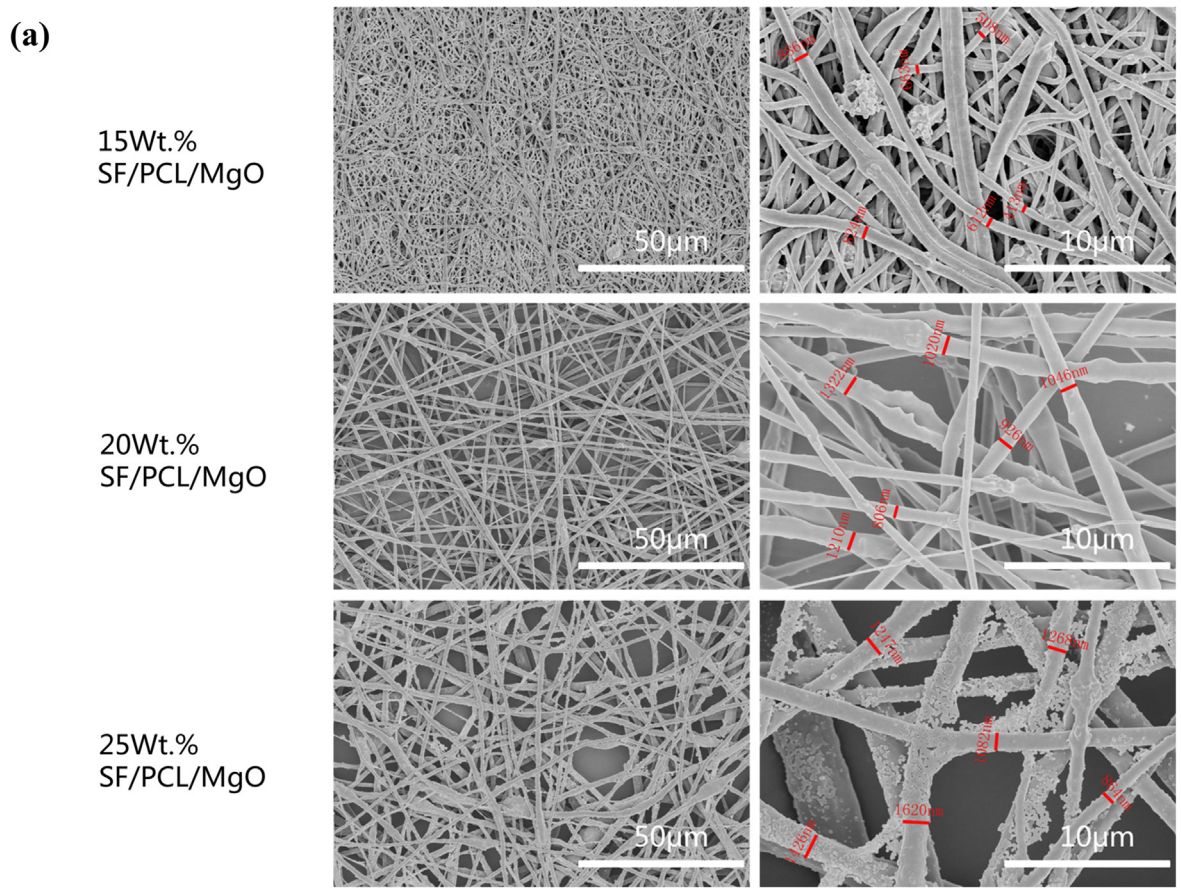

(b)

Samples	15Wt.% SF/PCL/MgO	20Wt.% SF/PCL/MgO	25Wt.% SF/PCL/MgO
Average diameter (nm)	651±165	1055±171	1251±240

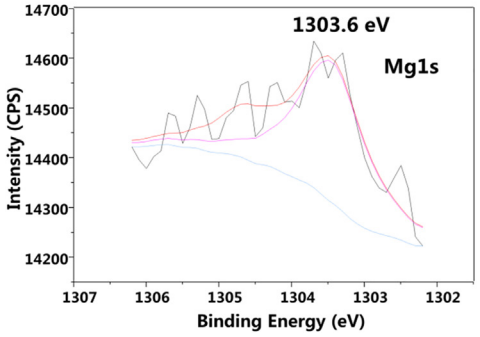

Fig. 1 Characterisation of SF/PCL/MgO membranes. (a) SEM images of the SF/PCL/MgO nanofibrous membranes with different ratios of MgO nanoparticles. (b) The average diameter of SF/PCL/MgO nanofibers with different ratios of MgO. (c) XPS wide scans of SF/PCL/MgO nanofibrous electrospinning membranes.

3.2. Hydrophilicity of the SF/PCL/MgO nanofibrous membranes

Water contact angle (WCA) data were obtained to demonstrate the hydrophilicity of the SF/PCL/MgO membranes (Fig. 2). No significant differences in WCA were observed between the SF/PCL/MgO and SF/PCL groups at 0 s ($p > 0.05$). The WCA of the SF/PCL membranes at 50 and 160 s was 43.2 ± 6.2 and 24.4 ± 7.6, respectively (Fig. 2**a**). With the incorporation of MgO, the SF/PCL/MgO membranes became increasingly hydrophilic and had WCA values of 27.6 ± 8.2 at 50 s ($p < 0.05$) (Fig. 2**b and c**). The water droplets were absorbed completely by the SF/PCL/MgO nanofibrous mats at 160 s. This result indicates that MgO helped improve the hydrophilic properties and wettability of the SF/PCL/MgO composite membranes.

3.3. Mg^{2+} Released from the SF/PCL/MgO composite membranes

The release curves of Mg^{2+} from 15 wt% SF/PCL/MgO, 20 wt % SF/PCL/MgO and 25 wt% SF/PCL/MgO electrospun membranes are shown in Fig. 3. A high percentage of released Mg^{2+} was detected when the composite membranes contained a large amount of MgO nanoparticles. The scaffolds showed a relative burst release in the first week. The range of 70%–80% Mg^{2+} was sustainably released from the composite membranes by the 15th day. Some Mg^{2+} was still released from

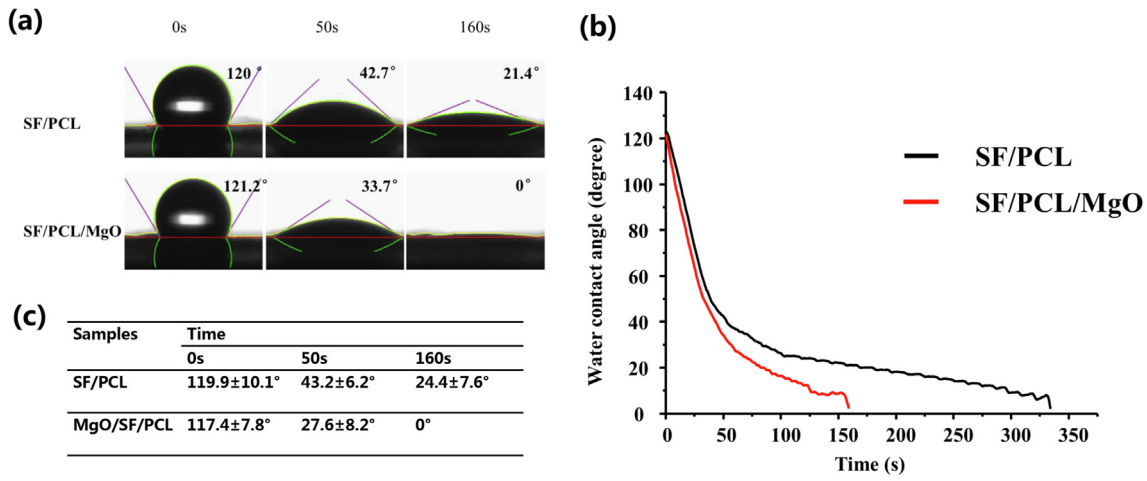

Samples	Time		
	0s	50s	160s
SF/PCL	119.9±10.1°	43.2±6.2°	24.4±7.6°
MgO/SF/PCL	117.4±7.8°	27.6±8.2°	0°

Fig. 2 Hydrophilicity of the SF/PCL/MgO electrospun membranes. (a–b) SF/PCL membrane without MgO nanoparticles incorporation completely absorbed the water droplets at 340 s, whereas the WCA reduced to 0 at 160 s with the incorporation of MgO. (c) No significant differences were found in the WCAs of all the groups at 0 s. The SF/PCL/MgO membranes exhibited a smaller WCA than the other groups at 50 s.

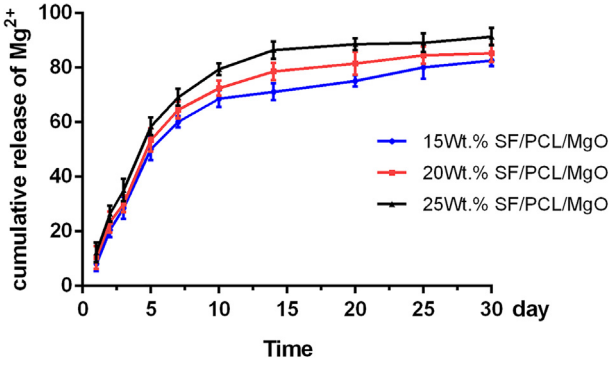

Fig. 3 Cumulative release profile of Mg^{2+} from the various SF/PCL/MgO composite membranes. The results are presented as the mean ± SD.

the composite membranes after a month of incubation. These results show that the composite membranes continuously released Mg^{2+} into the external medium.

3.4. Biocompatibility of nanofibrous SF/PCL/MgO membranes

The cytotoxicity of the SF/PCL/MgO and SF/PCL membrane extracts was examined by seeding pre-osteoblast MC3T3-E1 cells onto different composite membranes and evaluating cell viability using CCK-8 assay. As shown in Fig. 4**a**, cell viability (OD value at 450 nm) was similar in all groups on days 2, 4 and 6 of seeding, and no significant differences were observed amongst the groups. The prepared SF/PCL/MgO and SF/PCL membranes exhibited satisfactory cytocompatibility.

3.5. MgO nanoparticles containing SF/PCL nanofibrous membranes promote the attachment of pre-osteoblasts

After co-culturing the SF/PCL/MgO and SF/PCL membranes with pre-osteoblasts for 3 and 10 days, SEM was used to examine the cell attachment on the electrospun membranes. Compared with the bare SF/PCL scaffold in Fig. 4**b**, more cells with larger and more extended morphologies were found attached onto the membrane with added MgO nanoparticles. Confocal fluorescence microscopy revealed the same tendency (Fig. 5). A well-spread cytoskeleton was observed in the SF/PCL/MgO membranes. Moreover, the nuclei of the cells with normal morphology were observed. The result implied that Mg^{2+} ions could help cells attach and adhere successfully onto the electrospun membranes.

3.6. SF/PCL nanofibrous scaffolds hybridized with MgO nanoparticles promotes the osteogenic differentiation of pre-osteoblasts

It has been reported in which alkaline phosphatase (ALP) enzymatic activity is linked to initial mineralization (Zhong and Chu, 2012). The results of ALP staining revealed that cells exposed to the extract of the electrospun membranes had higher ALP activity than those of the control group on days 5 and 10 of co-culturing. The ALP activity of the MC3T3-E1 cells was significantly enhanced by culturing these cells in the extract of the SF/PCL/MgO electrospun membranes (Fig. 6**a and d**). Mineralisation associated with the osteogenic differentiation of cells was evaluated by alizarin red S staining (Arun Kumar et al., 2015). Fig. 6**b** and **e** showed that a larger positive region for mineral deposition was found in the SF/PCL/MgO and SF/PCL electrospun membranes in comparison with the culture plate seeded with cells. Cell matrix mineralisation was significantly elevated after 21 days of co-culturing with the SF/PCL/MgO extract in comparison with co-culturing with the SF/PCL membrane. It is indicated in Fig. 6**c** that positive-stained mineralised nodules were observed on the membranes when osteogenic differentiation and mineralisation of MC3T3-E1 cells occurred. Conversely, no calcified nodules were observed on the membranes without cell inoculation. This phenomenon means that the electrospun membrane did not adsorb dye compounds in itself.

To further confirm the effects of the SF/PCL/MgO composite membranes on the osteogenic differentiation of MC3T3-E1 cells, the expressions of osteogenic differentiation

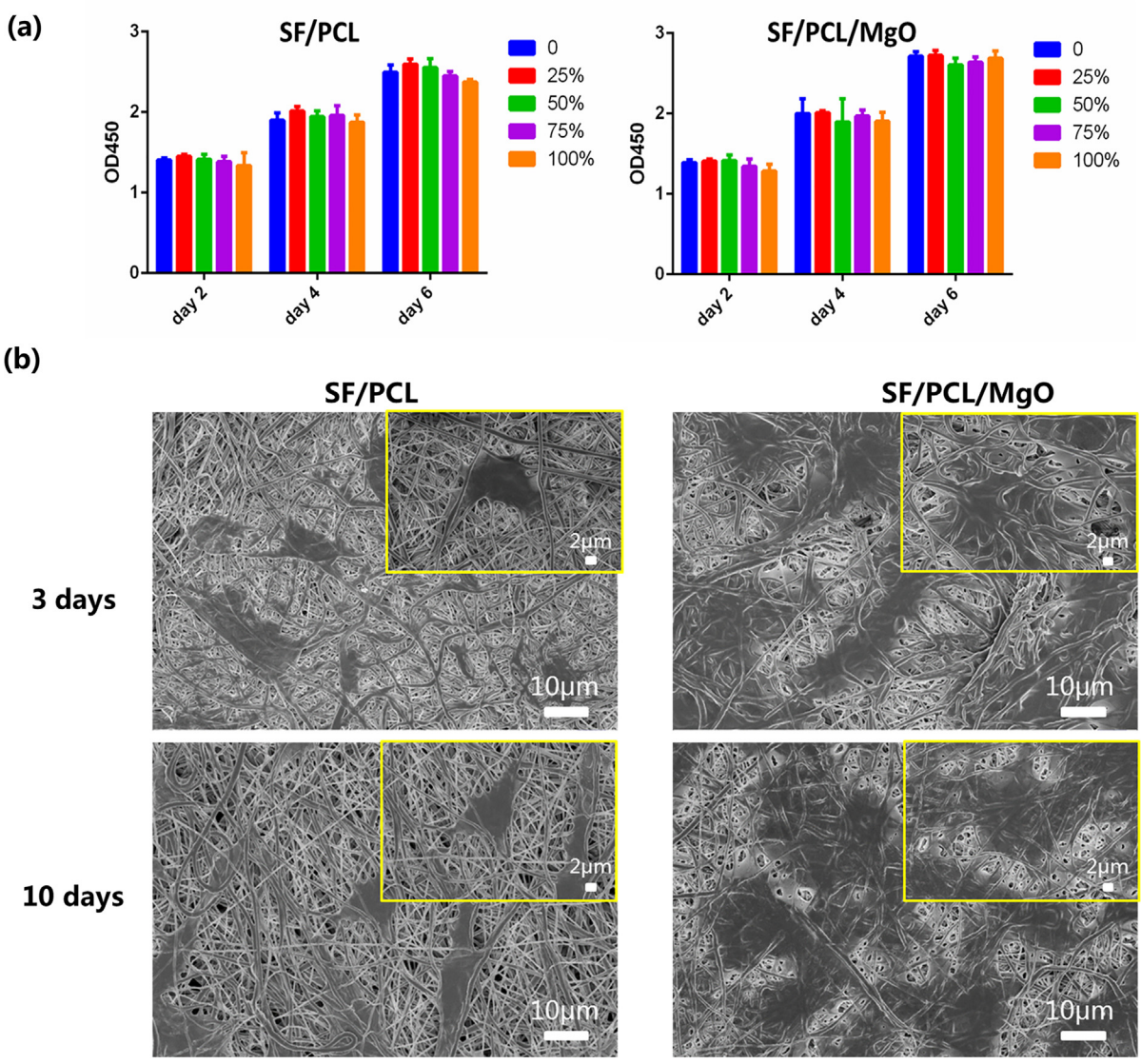

Fig. 4 In vitro cell biocompatibility study and cell adhesion of the SF/PCL and SF/PCL/MgO electrospun membranes. (a) CCK-8 assay was performed after 2, 4 and 6 days of culturing MC3T3-E1 on the different composite membranes. (b) SEM images of SF/PCL and SF/PCL/MgO membranes cultured with MC3T3-E1 cells for 3 and 10 days.

makers, including BMP-2, OCN, ALP and RUNX-2, were analysed by real-time PCR (Fig. 6**f**). Relative to the control group, BMP2 showed nearly 6.4-fold increased expression for the SF/PCL/MgO group on day 7, and OCN, ALP and RUNX2 showed 4.4-fold, 3.1-fold and 4.5-fold higher expression, respectively. The higher expression of these osteogenic differentiation-related genes in comparison with that of the SF/PCL group was observed in the cells cultured in the presence of the SF/PCL/MgO membrane. Therefore, the presence of MgO nanoparticles endowed the SF/PCL/MgO electrospun membranes with a strong capability to promote the osteogenic differentiation of pre-osteoblasts.

3.7. SF/PCL/MgO nanofibrous membranes for in vivo bone regeneration

To assess the feasibility of the designed scaffolds, the membranes were implanted in rat calvaria **(**Fig. 7**a)**, and the defects were correspondingly characterised after 4, 8 and 12 weeks. Fig. 7**b** shows the bone regeneration results of reconstructed micro-CT 3D models. The defects in the control group were poorly healed and presented a large uncovered area during the entire period of healing. The SF/PCL group showed better bone regeneration than the control group did (Fig. 7**b**). The defects covered by the SF/PCL/MgO membrane were almost fully bridged by the newly-formed bone tissue after 12 weeks of operation. The corresponding BV/TV values in the defect areas were calculated, and the data of the SF/PCL/MgO group were significantly higher than those of the two other groups (Fig. 7**c**).

New bone formation was further confirmed histologically by H&E and Masson's trichrome staining (Figs. 8 and 9). The defect areas in the control group were dominantly filled with fibrous tissues with no sign of new bone formation from 4 weeks to 12 weeks post-operation. By contrast, newly formed bone tissue was observed in the SF/PCL and SF/PCL/MgO

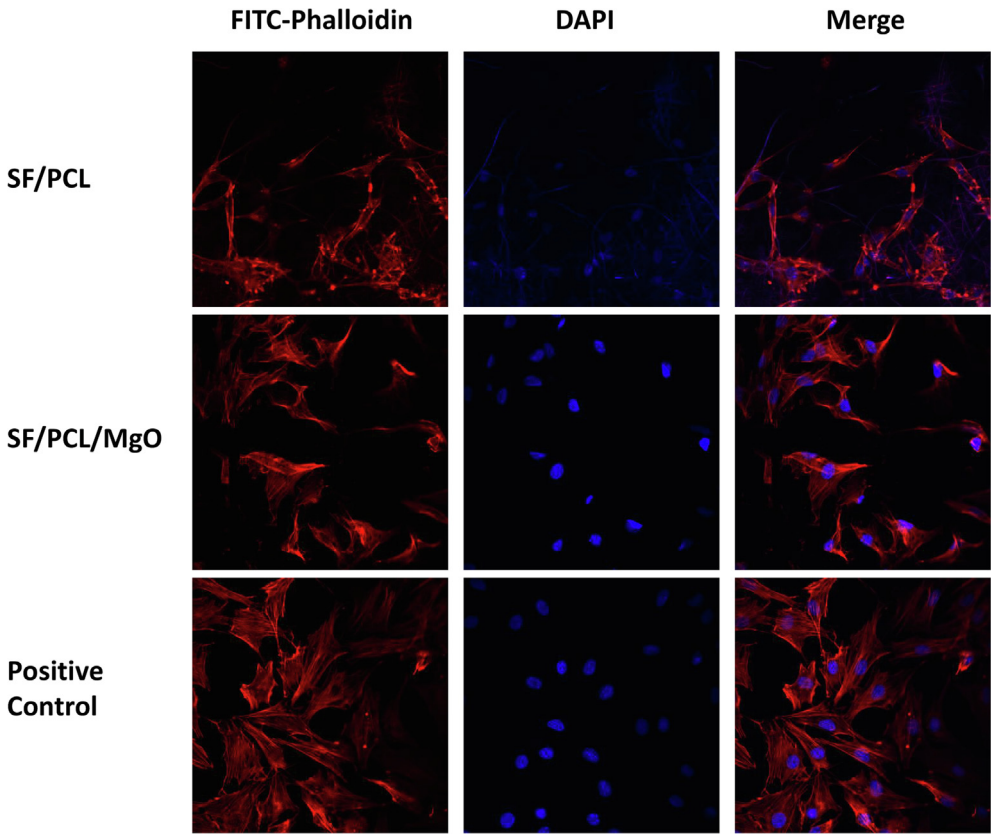

Fig. 5 Confocal fluorescence microscopy observation of pre-osteoblasts on the electrospun membranes.

groups. More mature collagen formation was observed in the SF/PCL/MgO group compared with the two other groups. The aforementioned results imply that the SF/PCL/MgO composite electrospun membranes that released Mg^{2+} favoured bone regeneration.

4. Discussion

Tissue engineering scaffolds coupled with the controlled release of bioactive substances represent a promising approach in large bone defect therapy and bone regeneration (Cheng et al., 2019). Magnesium is one of the essential elements in our body and plays vital roles in regulating the body's metabolism (O'Neill et al., 2018). Mg is regarded as an ideal implantation material for bone defect repair because it is biodegradable in vivo and possesses a balance between strength and degradation. In vivo investigations have shown that Mg alloys enhance bone regeneration (Yoshizawa et al., 2015). However, the degradation of Mg alloys is always coupled with the uncontrolled release of hydrogen gas and an alkaline environment, factors which hinder bone regeneration. One method to solve the problem involves introducing Mg^{2+} into a sustained-release system.

Accordingly in this study, a composite SF/PCL scaffold containing MgO nanoparticles was prepared via electrospinning technology to stimulate bone regeneration. MgO nanoparticles at different concentrations (15 wt%, 20 wt% and 25 wt%) was incorporated into the SF/PCL scaffold. The MgO ratio exerted certain effects on the physical properties of the composite scaffold. The SEM results showed that 20 wt% MgO SF/PCL had suitable porous structures. Low MgO nanoparticles concentrations caused irregular fibre morphology, whereas high MgO concentrations led to particle agglomeration in the electrospun membrane.

Nanofibre diameter is a vital parameter of synthetic membranes. As shown in our previous study, the average diameter of $(SF/PCL)_{4:1}$ membrane (0% group) was 337 ± 44 nm (Cheng et al., 2018). In composite SF/PCL/MgO blends, fibre diameters increased with increased MgO concentration; all diameters exceeded those of the 0% MgO group. The increased fibre diameter could be possibly ascribed to the formation of nano-MgO agglomerates, significantly hindered the elongation of the fibres during electrospinning. Eletrospun membranes offer an ideal fibrillar porous structure for cell and osteoconduction. Evidence on cellular biological responses being influenced by fibre diameter is emerging. Terranova et al. showed that the proliferation of MC3T3-E1 cells, seeded onto fibres with diameters ranging within 0.14–2.1 μm and 1–4.5 μm, increased with increased fibre diameters (Terranova et al., 2016). Badami et al. found the same trend in that MC3T3-E1 cells seem to have a greater cell density on fibres with larger diameters (Badami et al., 2006). In the present work, the adhesion of MC3T3-E1 cells onto SF/PCL membranes with thinner fibres and SF/PCL/MgO fibres with larger diameters were investigated. SEM and confocal fluorescence microscopy demonstrated that the MgO-loaded SF/PCL membrane had better attraction to pre-osteoblasts than the other scaffolds, an outcome that is consistent with those of previous literature (Kim et al., 2017). The greater number of cells spread

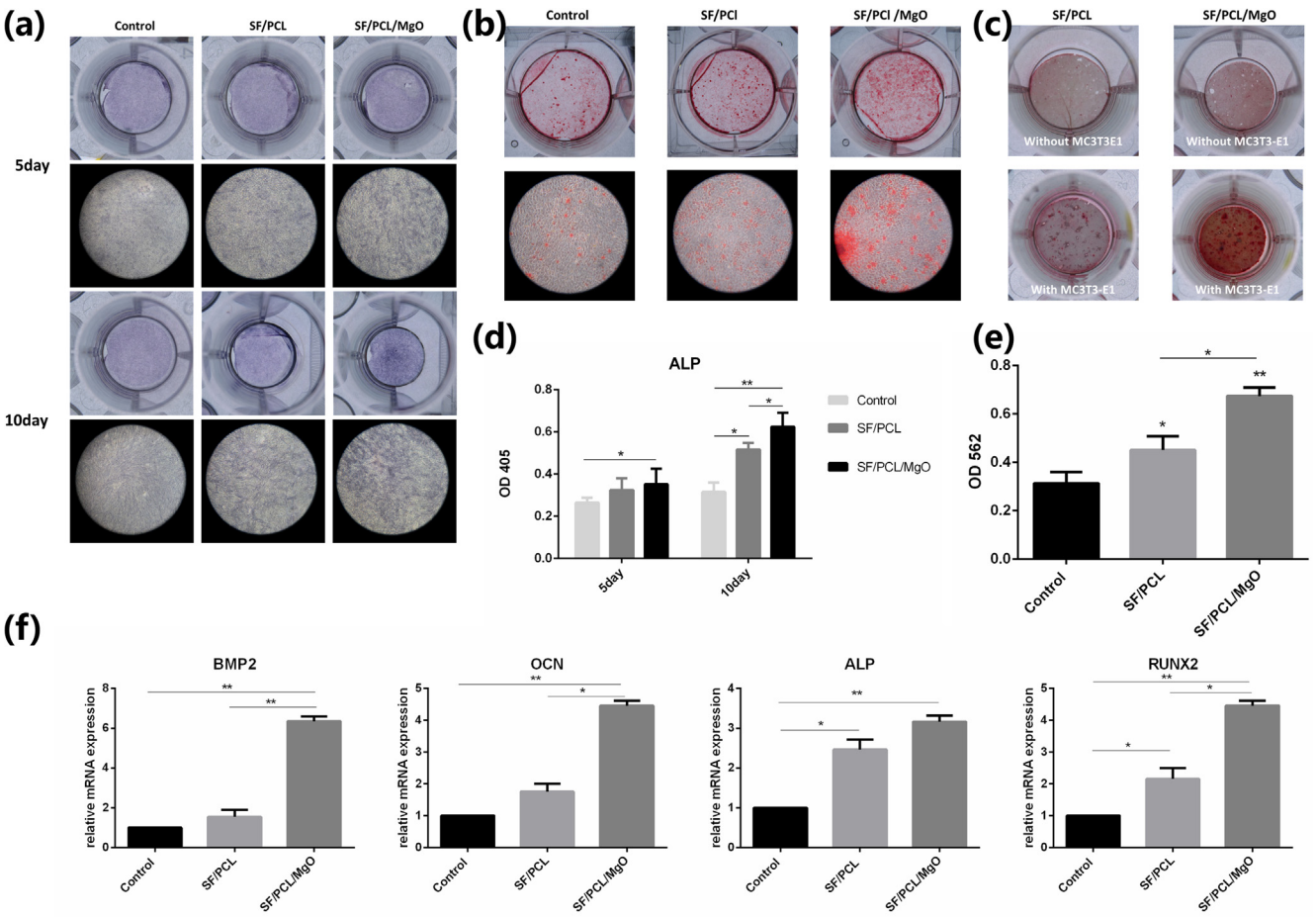

Fig. 6 In vitro osteogenesis capability of the electrospun membranes. (a) ALP staining of MC3T3-E1 cells incubated with the extract from the SF/PCL and SF/PCL/MgO membranes after 5 and 10 days of osteoinduction. (b) Alizarin red S staining of MC3T3-E1 cells cultured with the extract from the SF/PCL and SF/PCL/MgO membranes. (c) Alizarin red S staining of the SF/PCL and SF/PCL/MgO membrane with or without MC3T3-E1 cell incubation. (d) Quantification of ALP activity. (e) Quantitative analysis of mineralisation nodes. (f) Expression of osteogenic genes BMP2, OCN, ALP and RUNX2 in MC3T3-E1 cells cultured with or without the extract of the SF/PCL and SF/PCL/MgO membranes for 21 days of osteoinduction. * $p < 0.05$, **$p < 0.01$.

throughout SF/PCL/MgO fibres was due primarily to the Mg addition and partly to the larger-diameter fibres enabling greater interconnected porosity and to the pore shape allowing more cells to penetrate the scaffolds.

Controlled release of Mg^{2+} was achieved by incorporating MgO nanoparticles into the SF/PCL scaffold. The release curves indicated that the electrospun membrane can release the loaded Mg^{2+} in a controlled manner. As shown by the cytotoxicity results, both of SF/PCL and MgO-loaded SF/PCL composite membranes had good biocompatibility, which means that the Mg^{2+} concentrations in the SF/PCL/MgO composite membranes were safe and had no adverse effects on cell survival.

The ALP activity, alizarin red S and real-time PCR results indicated that SF/PCL was conducive to promoting osteoblast differentiation, which confirms the results of previously published studies (Cheng et al., 2018). Moreover, the cells seeded with the SF/PCL/MgO membranes extracts had the highest ALP activity, osteogenic markers and mineralised nodules. Numerous studies have shown that Mg^{2+} can promote osteogenic differentiation of MC3T3-E1 cells (Wu et al., 2015; Diaz-Tocados et al., 2017;7.). This fact may be attributed to the unknown synergistic effects of the SF/PCL membrane and Mg^{2+} on the differentiation of pre-osteoblasts.

To assess the feasibility of the designed scaffolds, the membranes were implanted in rat calvaria, and the defects were correspondingly characterised after 4, 8 and 12 weeks. Radiographic and histological analyses revealed that more new bone tissues were present in the group of the SF/PCL/MgO scaffold than in the others. With Mg^{2+} release from the scaffolds, the osteoblasts adhered to the SF/PCL/MgO membrane, differentiated and promoted new bone formation. Given that in vivo bone formation is much more complex than the in vitro counterpart, the local Mg^{2+} concentration was difficult to estimate. However, comparison of the groups indicated that Mg^{2+} was helpful for new bone formation.

Electrospun nanofibres can serve as ideal bone-tissue engineering scaffolds because of their large specific surface, architectural similarity to the natural extracellular matrix (ECM), and ease of functionalization. However, conventional electrospun fibrous membranes consist entirely of closed-packed fibres. In most cases, these fibres provide a superficial porous

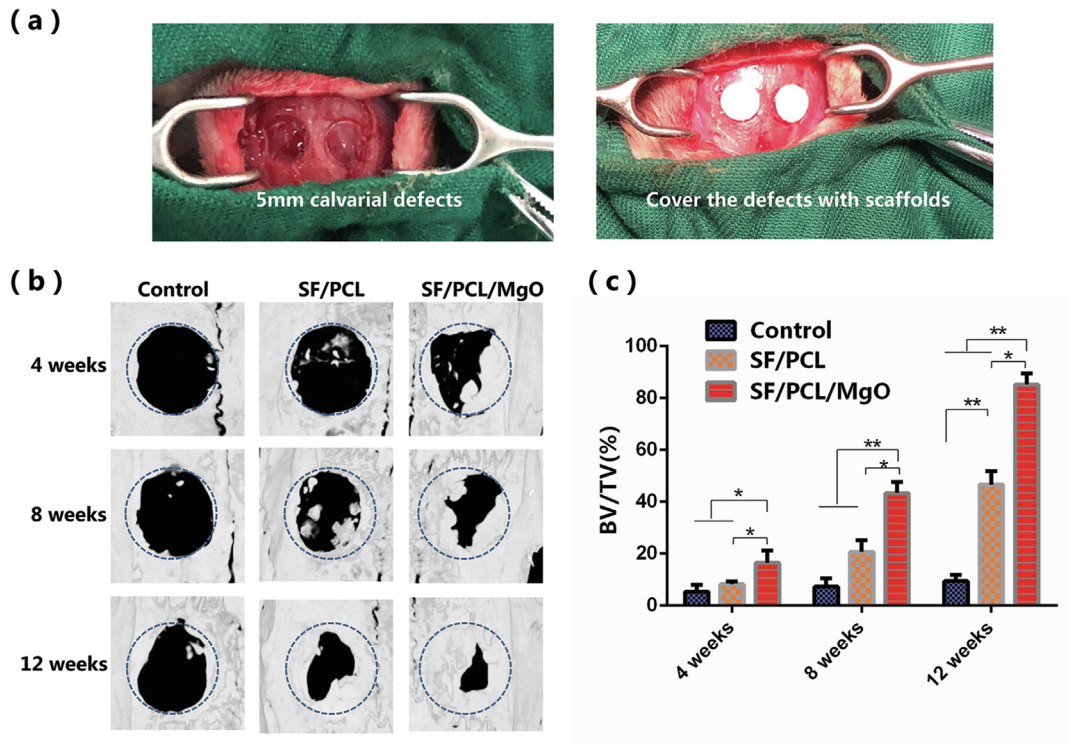

Fig. 7 In vivo radiologic examination of bone regeneration at rat calvaria defects. (a) Optical image of the rat calvarial defects (b) Reconstructed 3D micro-CT images of the rat calvaria defects implanted with SF/PCL and SF/PCL/MgO membranes. (c) Quantitative analysis of the regenerated bone in values of BV/TV for the SF/PCL, SF/PCL/MgO and control groups. * $p < 0.05$, ** $p < 0.01$.

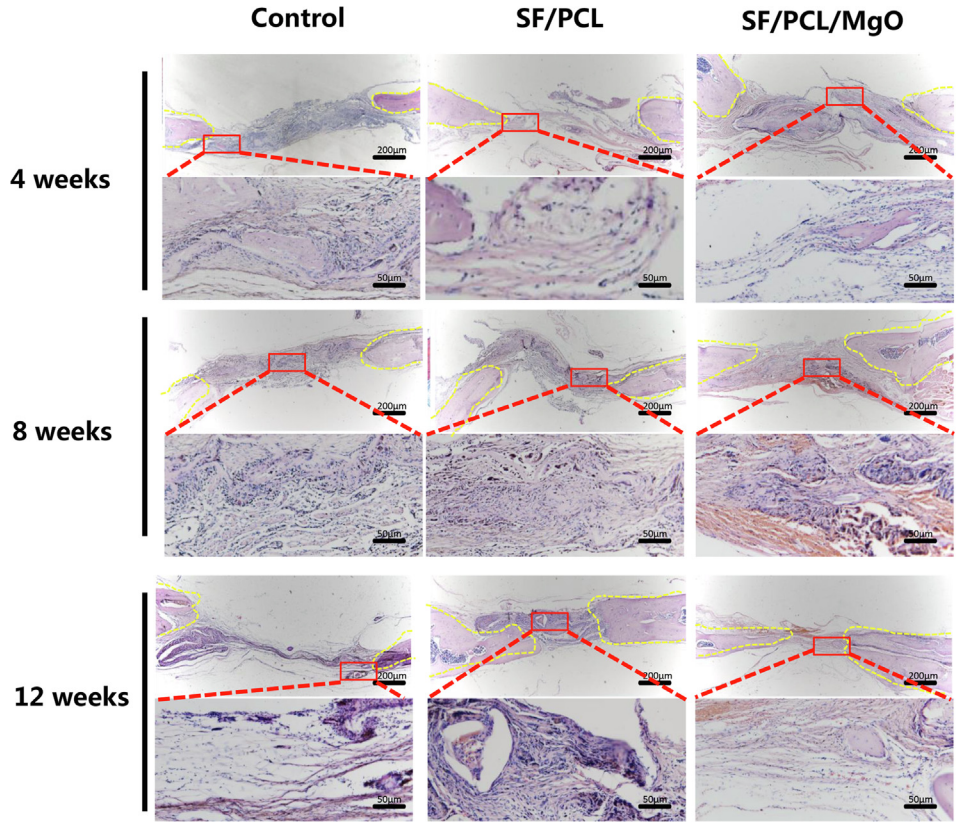

Fig. 8 H&E staining evaluation of the regeneration of bone defects in the SF/PCL, SF/PCL/MgO and control groups at 4, 8 and 12 weeks post-operation.

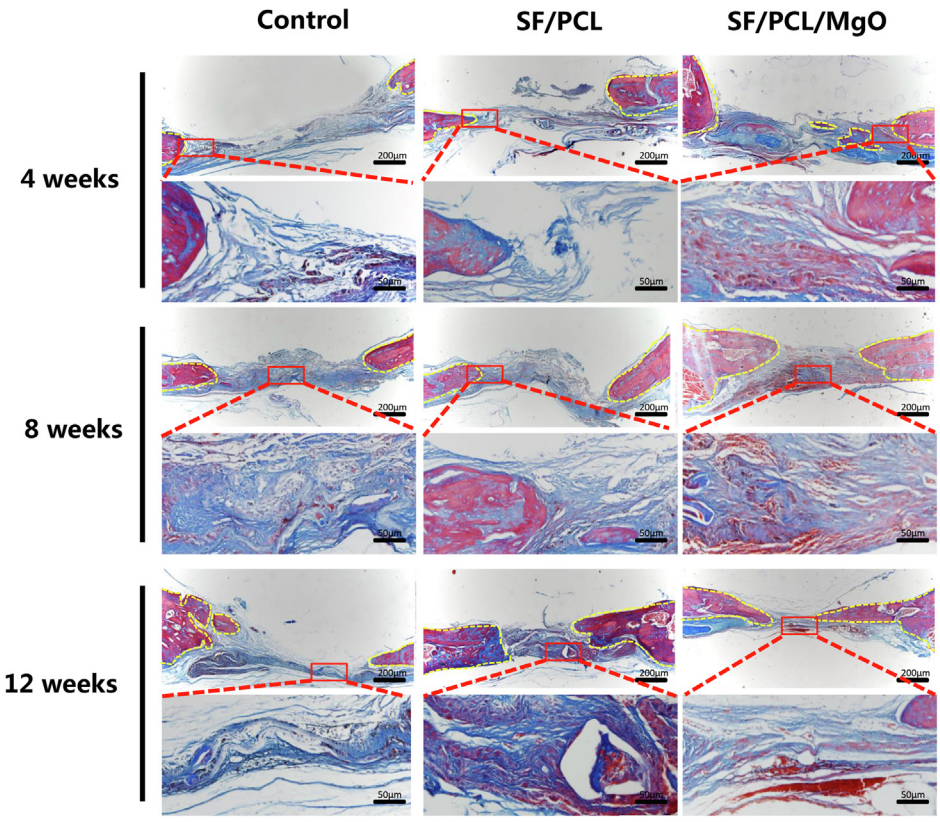

Fig. 9 Masson's trichrome staining for evaluation of the regeneration of bone defects in the SF/PCL, SF/PCL/MgO and control groups at 4, 8 and 12 weeks post-operation. The yellow dotted line indicates the boundary of newly formed bone tissue.

structure. With decreased fibre diameter from microscale to nanoscale, the porous structure becomes smaller. Traditional electrospun nanofibrous scaffolds present 2D surfaces lacking the necessary large pores for penetration and migration of cells on the electrospun matrix, in contrast to a 3D environment which more closely mimics the ECM (Lin et al., 2019; Jun et al., 2018). Moreover, electrospinning is a complex hydrodynamic atomization process dependent on numerous variable parameters, especially an unpredictable electrified jet (Bhardwaj and Kundu, 2010). Accordingly, most conventional electropsun nanofibres come with a disorganized nanofibre orientation and chaotic pattern designing. The ECM of various tissues consists of aligned protein fibrils and bundles with many biomedical applications that would benefit from aligned nanofibre assemblies (Chew et al., 2006). Hence, a great demand exists for the production of nanofibrous scaffolds with complex nanostructures and multidimensional architecture. Attempts have been made to fabricate complex 3D multiscale fibrous scaffolds with desirable microstructures and apply them to tissue engineering. (Asencio et al., 2018; Chen et al., 2017). Further studies on fibrous scaffolds are ongoing, with the aim of achieving efficient tissue engineering.

5. Conclusion

In summary, the control release of Mg^{2+} were successfully achieved by incorporating MgO nanoparticles into SF/PCL-based electrospun membranes that acted as efficient osteoinductive and osteoconductive platforms. The Mg^{2+}-containing SF/PCL scaffolds promoted the adherence and osteogenic differentiation of pre-osteoblasts. Therefore, this work represents a facile approach to the fabrication of a functional tissue engineering scaffold. And the currently designed magnesium-containing SF/PCL composite membrane can be used as a potential candidate for bone regeneration therapy.

Acknowledgements

This work was supported by Natural Science Foundation of China (No. 51873157, 81800943, and 81771051) and was partially supported by the Natural Science Foundation of Hubei Province of China (No.2018CFB497) and the Fundamental Research Funds for the Central Universities of China (no. 2042019kf0120).

References

Adhikari, U., An, X., Rijal, N., Hopkins, T., Khanal, S., Chavez, T., et al, 2019. Embedding magnesium metallic particles in polycaprolactone nanofiber mesh improves applicability for biomedical applications. Acta Biomater.

Aksoy, S., Caglar, Y., Ilican, S., Caglar, M., 2012. Sol–gel derived Li–Mg co-doped ZnO films: preparation and characterization via XRD, XPS FESEM. J. Alloys Compounds 512, 171–178.

Arun Kumar, R., Sivashanmugam, A., Deepthi, S., Iseki, S., Chennazhi, K.P., Nair, S.V., et al, 2015. Injectable chitin-poly(ε-caprolactone)/nanohydroxyapatite composite microgels prepared by simple regeneration technique for bone tissue engineering. ACS Appl. Mater. Interfaces.

Asencio, I.O., Mittar, S., Sherborne, C., Raza, A., Claeyssens, F., MacNeil, S., 2018. A methodology for the production of micro-

fabricated electrospun membranes for the creation of new skin regeneration models. J. Tissue Eng 9. 2041731418799851-.
Badami, A.S., Kreke, M.R., Thompson, M.S., Riffle, J.S., Goldstein, A.S., 2006. Effect of fiber diameter on spreading, proliferation, and differentiation of osteoblastic cells on electrospun poly(lactic acid) substrates. Biomaterials 27, 596–606.
Bhardwaj, N., Kundu, S.C., 2010. Electrospinning: a fascinating fiber fabrication technique. Biotechnol. Adv. 28, 325–347.
Bhattacharjee, P., Kundu, B., Naskar, D., Kim, H.W., Maiti, T.K., Bhattacharya, D., et al, 2017. Silk scaffolds in bone tissue engineering: an overview. Acta Biomater. 63, 1–17.
Burmester, A., Willumeit-Romer, R., Feyerabend, F., 2017. Behavior of bone cells in contact with magnesium implant material. J. Biomed. Mater. Res. B Appl. Biomater. 105, 165–179.
Castiglioni, S. et al, 2013. Magnesium and osteoporosis: current state of knowledge and future research directions. Nutrients 5, 3022–3033.
Chen, H., Malheiro, A.B.F.B., van Blitterswijk, C., Mota, C., Wieringa, P.A., Moroni, L., 2017. Direct writing electrospinning of scaffolds with multidimensional fiber architecture for hierarchical tissue engineering. ACS Appl. Mater. Interfaces 9, 38187–38200.
Chen, J., Zhan, Y., Wang, Y., Han, D., Tao, B., Luo, Z., et al, 2018. Chitosan/silk fibroin modified nanofibrous patches with mesenchymal stem cells prevent heart remodeling post-myocardial infarction in rats. Acta Biomater. 80, 154–168.
Cheng, G., Davoudi, Z., Xing, X., Yu, X., Cheng, X., Li, Z.B., et al, 2018. Advanced silk fibroin biomaterials for cartilage regeneration. ACS Biomater. Sci. Eng. 4, 2704–2715.
Cheng, G., Chen, J., Wang, Q., Yang, X., Cheng, Y., Li, Z., et al, 2018. Promoting osteogenic differentiation in pre-osteoblasts and reducing tibial fracture healing time using functional nanofibers. Nano Res. 11, 3658–3677.
Cheng, G., Yin, C., Tu, H., Jiang, S., Wang, Q., Zhou, X., et al, 2019. Controlled co-delivery of growth factors through layer-by-layer assembly of core-shell nanofibers for improving bone regeneration. ACS Nano 13, 6372–6382.
Chew, S.Y., Wen, Y., Dzenis, Y., Leong, K.W., 2006. The role of electrospinning in the emerging field of nanomedicine. Curr. Pharm. Des. 12, 4751–4770.
Choi, J.H., Kim, D.K., Song, J.E., Oliveira, J.M., Reis, R.L., Khang, G., 2018. Silk fibroin-based scaffold for bone tissue engineering. In: Chun, H.J., Park, K., Kim, C.-.H., Khang, G. (Eds.), Novel Biomaterials for Regenerative Medicine. Springer Singapore, Singapore, pp. 371–387.
Diaz-Tocados, J.M., Herencia, C., Martinez-Moreno, J.M., Montes de Oca, A., Rodriguez-Ortiz, M.E., Vergara, N., et al, 2017;7.. Magnesium Chloride promotes Osteogenesis through Notch signaling activation and expansion of Mesenchymal Stem Cells. Sci. Rep.
Farokhi, M., Mottaghitalab, F., Reis, R.L., Ramakrishna, S., Kundu, S.C., 2020. Functionalized silk fibroin nanofibers as drug carriers: advantages and challenges. J. Control. Release 321, 324–347.
Fernandez de Grado, G., Keller, L., Idoux-Gillet, Y., Wagner, Q., Musset, A.-M., Benkirane-Jessel, N., et al, 2018. Bone substitutes: a review of their characteristics, clinical use, and perspectives for large bone defects management. J. Tissue Eng. 9. 2041731418776819-.
Grober, U., Schmidt, J., Kisters, K., 2015. Magnesium in Prevention and Therapy. Nutrients 7, 8199–8226.
Haider, A., Haider, S., Kang, I.-K., 2018. A comprehensive review summarizing the effect of electrospinning parameters and potential applications of nanofibers in biomedical and biotechnology. Arabian J. Chem. 11, 1165–1188.
Jun, I., Han, H.-S., Edwards, R.J., Jeon, H., 2018. Electrospun fibrous scaffolds for tissue engineering: viewpoints on architecture and fabrication. Int. J. Mol. Sci. 19.
Kim, K.J., Choi, S., Sang Cho, Y., Yang, S.J., Cho, Y.S., Kim, K.K., 2017. Magnesium ions enhance infiltration of osteoblasts in scaffolds via increasing cell motility. J. Mater. Sci. – Mater. Med. 28, 96.
Kim, B.S., Park, K.E., Kim, M.H., You, H.K., Lee, J., Park, W.H., 2015. Effect of nanofiber content on bone regeneration of silk fibroin/poly(epsilon-caprolactone) nano/microfibrous composite scaffolds. Int. J. Nanomed. 10, 485–502.
Kim, J.A., Yun, H.S., Choi, Y.A., Kim, J.E., Choi, S.Y., Kwon, T.G., et al, 2018. Magnesium phosphate ceramics incorporating a novel indene compound promote osteoblast differentiation in vitro and bone regeneration in vivo. Biomaterials 157, 51–61.
Lauthe, O., Soubeyrand, M., Babinet, A., Dumaine, V., Anract, P., 2018. Biau DJ. The indications and donor-site morbidity of tibial cortical strut autografts in the management of defects in long bones. The Bone Joint J. 100-B, 667–674.
Lin, W., Chen, M., Qu, T., Li, J., Man, Y., 2019. Three-dimensional electrospun nanofibrous scaffolds for bone tissue engineering. J. Biomed. Mater. Res. Part B: Appl. Biomater.
Lin, S., Yang, G., Jiang, F., Zhou, M., Yin, S., Tang, Y., et al, 2019. A magnesium-enriched 3D culture system that mimics the bone development microenvironment for vascularized bone regeneration. Adv. Sci. 6, 1900209.
Noviana, D., Paramitha, D., Ulum, M.F., Hermawan, H., 2016. The effect of hydrogen gas evolution of magnesium implant on the postimplantation mortality of rats. J. Orthopaedic Trans. 5, 9–15.
O'Neill, E., Awale, G., Daneshmandi, L., Umerah, O., Lo, K.W., 2018. The roles of ions on bone regeneration. Drug Discov. Today 23, 879–890.
Roddy, E., DeBaun, M.R., Daoud-Gray, A., Yang, Y.P., Gardner, M. J., 2018. Treatment of critical-sized bone defects: clinical and tissue engineering perspectives. Eur. J. Orthop. Surg. Traumatol. 28, 351–362.
Rödel, M., Baumann, K., Groll, J., Gbureck, U., 2018. Simultaneous structuring and mineralization of silk fibroin scaffolds. J. Tissue Eng. 9. 2041731418788509-.
Roh, H.S., Lee, C.M., Hwang, Y.H., Kook, M.S., Yang, S.W., Lee, D., et al, 2017. Addition of MgO nanoparticles and plasma surface treatment of three-dimensional printed polycaprolactone/hydroxyapatite scaffolds for improving bone regeneration. Mater. Sci. Eng. C, Mater. Biol. Appl. 74, 525–535.
Seitz, J.M. et al, 2014. Magnesium degradation products: effects on tissue and human metabolism. J. Biomed. Mater. Res. Part A 102, 3744–3753.
Suryavanshi, A., Khanna, K., Sindhu, K.R., Bellare, J., Srivastava, R., 2017. Magnesium oxide nanoparticle-loaded polycaprolactone composite electrospun fiber scaffolds for bone–soft tissue engineering applications:in-vitroandin-vivoevaluation. Biomed. Mater. 12, 055011.
Terranova, L., Mallet, R., Perrot, R., Chappard, D., 2016. Polystyrene scaffolds based on microfibers as a bone substitute; development and in vitro study. Acta Biomater. 29, 380–388.
Winkler, T., Sass, F.A., Duda, G.N., Schmidt-Bleek, K., 2018. A review of biomaterials in bone defect healing, remaining shortcomings and future opportunities for bone tissue engineering: The unsolved challenge. Bone Joint Res 7, 232–243.
Wu, L., Feyerabend, F., Schilling, A.F., Willumeit-Romer, R., Luthringer, B.J.C., 2015. Effects of extracellular magnesium extract on the proliferation and differentiation of human osteoblasts and osteoclasts in coculture. Acta Biomater. 27, 294–304.
Yin, M., Xu, F., Ding, H., Tan, F., Song, F., Wang, J., 2015. Incorporation of magnesium ions into photo-crosslinked alginate hydrogel enhanced cell adhesion ability. J. Tissue Eng. Regen. M 9, 1088–1092.
Yoshizawa, S., Chaya, A., Verdelis, K., Bilodeau, E.A., Sfeir, C., 2015. An in vivo model to assess magnesium alloys and their biological effect on human bone marrow stromal cells. Acta Biomater. 28, 234–239.

Yu, W., Li, R., Long, J., Chen, P., Hou, A., Li, L., et al, 2019. Use of a three-dimensional printed polylactide-coglycolide/tricalcium phosphate composite scaffold incorporating magnesium powder to enhance bone defect repair in rabbits. J. Orthopaedic Transl. 16, 62–70.

Yuan, Z., Wei, P., Huang, Y., Zhang, W., Chen, F., Zhang, X., et al, 2019. Injectable PLGA microspheres with tunable magnesium ion release for promoting bone regeneration. Acta Biomater. 85, 294–309.

Zhang, L., Pei, J., Wang, H., Shi, Y., Niu, J., Yuan, F., et al, 2017. Facile Preparation of Poly(lactic acid)/Brushite Bilayer Coating on Biodegradable Magnesium Alloys with Multiple Functionalities for Orthopedic Application. ACS Appl. Mater. Interfaces 9, 9437–9448.

Zhang, Y., Xu, J., Ruan, Y.C., Yu, M.K., O'Laughlin, M., Wise, H., et al, 2016. Implant-derived magnesium induces local neuronal production of CGRP to improve bone-fracture healing in rats. Nat. Med. 22, 1160–1169.

Zhong, C., Chu, C.C., 2012. Biomimetic mineralization of acid polysaccharide-based hydrogels: towards porous 3-dimensional bone-like biocomposites. J. Mater. Chem. 22, 6080–6087.